Supplementary Information for

Real-time measurement of non-Hermitian Landau-Zener tunneling near band crossings

Lange Zhao[a,#], Shulin Wang[a,e,#], Chengzhi Qin[a,#], Bing Wang[a,*], Han Ye[a], Weiwei Liu[a], Stefano Longhi[b,c,*] and Peixiang Lu[a,d,*]

[a]Wuhan National Laboratory for Optoelectronics and School of Physics, Huazhong University of Science and Technology, Wuhan 430074, China.

[b]Dipartimento di Fisica, Politecnico di Milano, Piazza Leonardo da Vinci 32, I-20133 Milano, Italy.

[c]IFISC (UIB-CSIC), Instituto de Fisica Interdisciplinary Sistemas Complejos, E-07122 Palma de Mallorca, Spain.

[d]Hubei Key Laboratory of Optical Information and Pattern Recognition, Wuhan Institute of Technology, Wuhan 430205, China.

[e]School of Physics, Southeast University, Nanjing 211189, China.

[#]These authors contributed equally to this work

[*]Corresponding authors:

B. W. (email: wangbing@hust.edu.cn),

S. L. (email: stefano.longhi@polimi.it),

P. L. (email: lupeixiang@hust.edu.cn).

Supplementary Note 1: Synthetic temporal lattices

In this section, the mapping of the light pulses dynamics in two coupled fiber loops to the light propagation in a synthetic temporal lattice is discussed. The dynamics of two coupled fiber loops with different length mentioned in main text can be mapped onto the mesh lattice with time steps m and spatial positions n,[46,48] as depicted in Fig. S1. The length difference between the long loop and short loop makes it possible to have a time delay when the pulses of the two paths interfere in the central optical coupler. Coupling the optical pulse sequence into one of the loops, after a period of evolution, there will be a pulse sequence in both loops, the pulse into the short loop is equivalent to the leftward propagation in the temporal mesh lattice (advance effect); the pulse into the long loop is equivalent to the rightward propagation in the temporal mesh lattice (delay effect). The above process is similar to discrete diffraction in a waveguide array, where the lateral spatial dimension corresponds to the evolution of the wave packet in the pulse sequence in the fiber loops; the vertical temporal dimension corresponds to the number of turns (number of loops) of the wave packet evolution in the fiber loops. In other words, the relative position of wave packets gives spatial indicators in the transverse dimension n. And each cycle is equivalent to one step of evolution in the figure below, using m as a marker. By adding intensity modulators and phase modulators into the loops, we can manipulate the light pulses in each node in mesh lattice. The effective electric field can be obtained by changing the parameters of phase modulators and the loss can be introduced into the mesh lattice by controlling the electric signal of intensity modulator in short loop.

The experimental realization of synthetic temporal photonic lattice is constructed by utilizing a couple fiber-loop circuit, as depicted in Fig. S2. The fiber loops are connected by a variable optical coupler (VOC) with each having a length of ~5 km, which implies a circulation time of ~25 μs for individual pulses. The loss caused by the passive optical devices can be compensated by the erbium-doped fiber amplifiers (EDFAs). The length difference of the fiber loops is ~20 m and thus the adjacent pulses manifest a time interval of ~100 ns. The short loop includes a phase modulator which is used to yield a phase difference of $2\phi(m)$ with that in the long loop. Therefore, a vector potential $A = -\phi(m)$ and a scalar potential $\phi(m)$ are generated in the temporal lattice. Note that the scalar potential has no effect on the evolution of wave packets. The arrangement produces exactly the same results as applying opposite phase modulations in the two loops. The incident pulse is converted to a Gaussian-like wave packet consisting of discrete pulses by using an intensity modulator (IM), which is driven by an arbitrary waveform generator (AWG). Each loop contains an IM to manipulate the loss rates of the system. By varying the voltage signals that drive the IM, the transmittance of IM can be reduced and the desired loss modulation is realized. In the aid of optical couplers, the pulses are exported into the

photodetectors which are connected with an oscilloscope. As the wave packet is injected into the fiber-loop circuit, the temporal waveforms in the short and long loops for each roundtrip can be recorded in real time.

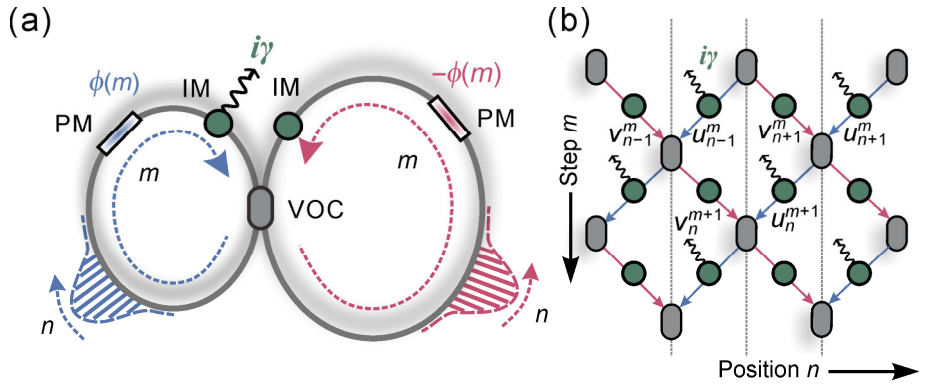

Fig. S1. A part of the temporal mesh lattice. The propagation in the fiber loops (a) maps onto a mesh lattice (b) of optical couplers and modulators. The grey rectangles indicate optical couplers. The green circles represent the intensity modulators. The curved arrows denote the loss introduced into the mesh lattice.

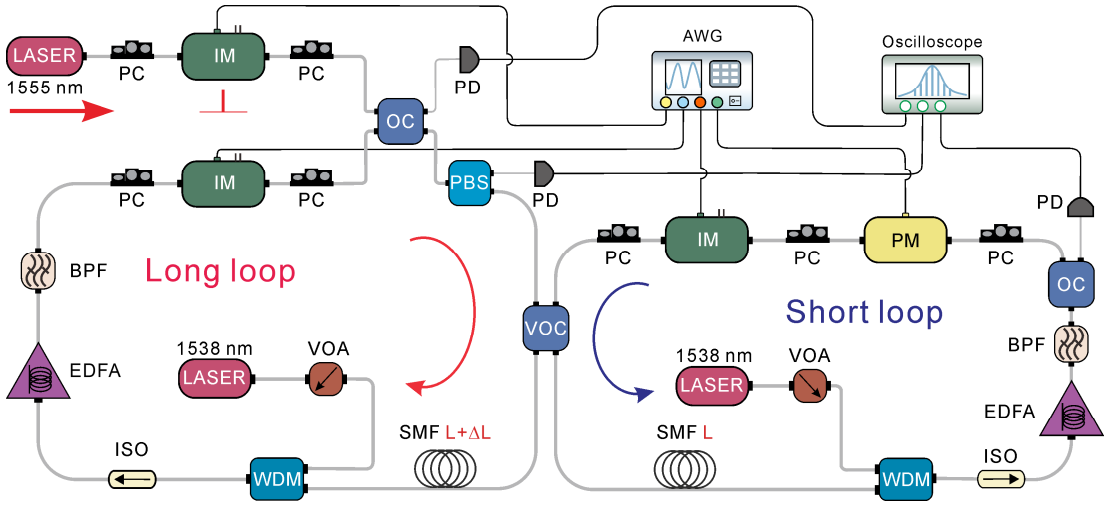

Fig. S2. Experimental setup. The gray lines indicate optical paths. The black lines represent the transmission of electric signals. PC, polarization controller; IM, intensity modulator; VOC, variable optical coupler; PD, photodiode; PBS, polarization beam splitter; SMF, single mode fiber; VOA, variable optical attenuator; WDM, wavelength division multiplexer; ISO, isolator; EDFA, erbium-doped fiber amplifier; BPF, band-pass filter; PM, phase modulator; OC, optical coupler; AWG, arbitrary waveform generator.

Supplementary Note 2: Experimental setup and measurement method

In this section, we shall derive the dispersion relation and eigenmodes of the dissipative synthetic temporal lattice. The propagation of the optical pulses in the fiber loops [Fig. S1(a)] can be mapped to a two-dimensional mesh lattice [Fig. S1(b)]. The time step and arriving time in a single loop are denoted by m and n, respectively, corresponding to the longitude and lateral dimensions in the mesh lattice. u_n^m and v_n^m represent the pulse amplitudes of the nth pulse at the mth time step in the short and long loops respectively. As shown in Fig. S1(b), considering the coupling of amplitudes before and after the coupler, we have

$$u_n^{m+1} = tu_{n+1}^m + rv_{n+1}^m, \quad v_n^{m+1} = tv_{n-1}^m + ru_{n-1}^m, \tag{S1}$$

with $t = \cos(\beta)$ and $r = i\sin(\beta)$ representing the direct and cross coupling coefficients of the optical pulses between the fiber rings, where β is the coupling angle characterizing the splitting ratio of the variable optical coupler. Then we have

$$\begin{cases} u_n^{m+1} = \cos(\beta)u_{n+1}^m + i\sin(\beta)v_{n+1}^m \\ v_n^{m+1} = i\sin(\beta)u_{n-1}^m + \cos(\beta)v_{n-1}^m \end{cases}. \tag{S2}$$

Considering the phase modulation imposed on the short and long rings as $\phi(m)$ and $-\phi(m)$, as well as the loss added on the short ring with the loss rate γ, the equation is rewritten as

$$\begin{cases} u_n^{m+1} = \cos(\beta)u_{n+1}^m e^{i\phi(m)-\gamma} + i\sin(\beta)v_{n+1}^m e^{-i\phi(m)} \\ v_n^{m+1} = i\sin(\beta)u_{n-1}^m e^{i\phi(m)-\gamma} + \cos(\beta)v_{n-1}^m e^{-i\phi(m)} \end{cases}. \tag{S3}$$

Another version of the equation can be expressed as

$$\begin{cases} u_n^{m+1} = [\cos(\beta)u_{n+1}^m + i\sin(\beta)v_{n+1}^m]\exp[i\phi(m)-\gamma] \\ v_n^{m+1} = [i\sin(\beta)u_{n-1}^m + \cos(\beta)v_{n-1}^m]\exp[-i\phi(m)] \end{cases}. \tag{S4}$$

From Eq. (S4), the transfer matrix between adjacent steps can be obtained, i.e.,

$$T = \begin{pmatrix} \cos(\beta)e^{i\phi(m)-\gamma} & i\sin(\beta)e^{i\phi(m)-\gamma} \\ i\sin(\beta)e^{-i\phi(m)} & \cos(\beta)e^{-i\phi(m)} \end{pmatrix}. \tag{S5}$$

Let us first assume $\phi(m) = 0$. The amplitudes of the Bloch modes with a specific Bloch momentum Q can be obtained by performing Fourier transform of the real-space amplitudes of u_n^m and v_n^m, i.e.,

$$\begin{cases} U_Q^m = \sum_n e^{iQn}u_n^m \\ V_Q^m = \sum_n e^{iQn}v_n^m \end{cases}. \tag{S6}$$

Inserting Eq. (S6) into Eq. (S4), we can obtain

$$\begin{cases} U_Q^{m+1} = e^{iQ}[\cos(\beta)U_Q^m + i\sin(\beta)V_Q^m]e^{-\gamma} \\ V_Q^{m+1} = e^{-iQ}[\cos(\beta)V_Q^m + i\sin(\beta)U_Q^m] \end{cases}, \tag{S7}$$

which can be rewritten as

$$\begin{pmatrix} U_Q^{m+1} \\ V_Q^{m+1} \end{pmatrix} = \begin{pmatrix} \cos(\beta)e^{iQ}e^{-\gamma} & i\sin(\beta)e^{iQ}e^{-\gamma} \\ i\sin(\beta)e^{-iQ} & \cos(\beta)e^{-iQ} \end{pmatrix} \begin{pmatrix} U_Q^m \\ V_Q^m \end{pmatrix}. \tag{S8}$$

The single-step time evolution operator can thus be defined as

$$\Gamma(Q) = \begin{pmatrix} \cos(\beta)e^{i(Q+i\gamma)} & i\sin(\beta)e^{i(Q+i\gamma)} \\ i\sin(\beta)e^{-iQ} & \cos(\beta)e^{-iQ} \end{pmatrix}. \tag{S9}$$

By solving the eigenvalue equation

$$\Gamma(Q)\begin{pmatrix} U \\ V \end{pmatrix} = e^{i\theta}\begin{pmatrix} U \\ V \end{pmatrix}, \tag{S10}$$

we can further obtain

$$\begin{vmatrix} \cos(\beta)e^{iQ}e^{-\gamma} - e^{i\theta} & i\sin(\beta)e^{iQ}e^{-\gamma} \\ i\sin(\beta)e^{-iQ} & \cos(\beta)e^{-iQ} - e^{i\theta} \end{vmatrix} = 0, \tag{S11}$$

which leads to

$$e^{2i\theta} - \cos(\beta)(e^{iQ}e^{-\gamma} + e^{-iQ})e^{i\theta} + e^{-\gamma} = 0. \tag{S12}$$

By denoting $\theta' = \theta - i\gamma/2$, $Q' = Q + i\gamma/2$, Eq. (S12) can be rewritten as

$$e^{2i\theta'} - 2\cos(\beta)\cos(Q')e^{i\theta'} + 1 = 0, \tag{S13}$$

which gives rise to the solution

$$\cos(\theta') = \cos(\beta)\cos(Q'). \tag{S14}$$

That is,

$$\cos(\theta - i\frac{\gamma}{2}) = \cos(\beta)\cos(Q + i\frac{\gamma}{2}). \tag{S15}$$

Equation (S15) gives rise to the final quasi-energy band structure

$$\theta_{\pm} = \pm\cos^{-1}[\cos(\beta)\cos(Q + i\frac{\gamma}{2})] + i\frac{\gamma}{2}. \tag{S16}$$

Then we derive the eigen modes. Equation (S10) can also be denoted as

$$\left(\frac{V}{U}\right)^2 - i\cot(\beta)(1 - e^{-2iQ}e^{\gamma})\left(\frac{V}{U}\right) - e^{-2iQ}e^{\gamma} = 0. \tag{S17}$$

Similarly, by denoting $Q' = Q + i\gamma/2$, the solution of Eq. (S17) is

$$\frac{V}{U} = e^{-iQ'}[\cot(\beta)\sin(Q') \pm \sqrt{\cot^2(\beta)\sin^2(Q') + 1}]. \tag{S18}$$

Further, by denoting $\sinh(\lambda) = \cot(\beta)\sin(Q')$, we have

$$\begin{cases} e^{\lambda} = \cot(\beta)\cdot\sin(Q') + \sqrt{1+\cot^2(\beta)\cdot\sin^2(Q')} \\ e^{-\lambda} = -\cot(\beta)\cdot\sin(Q') + \sqrt{1+\cot^2(\beta)\cdot\sin^2(Q')} \end{cases}. \tag{S19}$$

As a result, the corresponding right and left eigenvectors can be expressed as

$$\begin{aligned} |\varphi_{\pm}\rangle &= \begin{pmatrix} U_{\pm} \\ V_{\pm} \end{pmatrix} = \frac{1}{\sqrt{1+\left|e^{\mp\lambda+\gamma/2}\right|^2}} \begin{pmatrix} 1 \\ \pm e^{\mp\lambda - iQ + \gamma/2} \end{pmatrix}, \\ |\chi_{\pm}\rangle &= \begin{pmatrix} \hat{U}_{\pm} \\ \hat{V}_{\pm} \end{pmatrix} = \frac{\sqrt{1+\left|e^{\mp\lambda+\gamma/2}\right|^2}}{2\cosh\lambda^*} \begin{pmatrix} e^{\pm\lambda^*} \\ \pm e^{-iQ-\gamma/2} \end{pmatrix}, \end{aligned} \tag{S20}$$

where $\lambda = \sinh^{-1}[\cot(\beta)\sin(Q+i\gamma/2)]$. Normalization has been assumed to satisfy the usual orthonormal relations $\langle\chi_{\pm}|\varphi_{\pm}\rangle = 1$ and $\langle\chi_{\mp}|\varphi_{\pm}\rangle = 0$ for left/right eigenvectors. Note that the right eigenvectors are not orthogonal in the non-Hermitian system.

The behavior of energy spectrum in complex plane is depicted in Fig. S3. The two energy bands are gapped[66] and display a spectral phase transition at $\gamma = \gamma_c$ with $\gamma_c = 2\cosh^{-1}[1/\cos(\beta)]$, where the system becomes gapless and an exceptional point (EP) occurs at the band touching point $Q = 0$. Interestingly, such a spectral phase transition can be described rather universally in terms of a NH extension of the Dirac equation where dissipation breaks Lorentz symmetry and is responsible for the appearance of the NH skin effect.[31,44] As the phase $\phi(m)$ is linearly ramped in time m, the instantaneous quasi energies and corresponding adiabatic eigenstates are obtained by the replacement $Q \to Q+\phi(m)$, so that the Bloch quasi momentum is spanned across the complex-energy gap and non-adiabatic transitions are possible. Clearly, the complex nature of the gap and non-orthogonality of adiabatic eigenstates influences the Landau-Zener (LZ) tunneling process. Figure S4 shows the overlap $\langle\varphi_{\mp}|\varphi_{\pm}\rangle$ between the two right eigenstates versus the Bloch momentum Q. For values away from the avoided crossing, the eigenstates are almost orthogonal, leading the system to behave in an essentially Hermitian way. For values around the avoided crossing, the non-Hermiticity is more apparent in the non-vanishing overlap of the eigenstates. The two adiabatic modes can be represented as $|\varphi_{\pm}\rangle = U_{\pm}|\varphi_s\rangle + V_{\pm}|\varphi_l\rangle$ in the diabatic basis, where $|\varphi_s\rangle = (1,0)^T$ and $|\varphi_l\rangle = (0,1)^T$ stand for the two bare modes in the short and long rings as they are uncoupled with each other (this occurs as $\beta \to 0$). In particular, the mode distributions in the adiabatic basis are almost equal to that in the diabatic basis far away from the band gap. For this reason, the incident wave packets are always initially prepared in the adiabatic basis, either for the measurement of the tunneling process in diabatic basis or for the measurement of the tunneling process in adiabatic basis. Figure S5 illustrates the mode distributions in different bases

for specific values of Bloch momentum Q. At the exceptional point i.e. for $Q = 0$ and $\gamma = \gamma_c$ with $\gamma_c = 2\cosh^{-1}[1/\cos(\beta)]$, the eigenvalues coalesce and their corresponding (adiabatic) eigenvectors become completely parallel. The critical value of parameter λ in Eq. (S20), i.e. when we approach the EP, is $\lambda_c = i\pi/2$; correspondingly, the denominator of normalization coefficient in left eigenvector, $\cosh(-i\pi/2)$ vanishes. This term with zero results in the ill-defined nature of the mode coefficients at EP in adiabatic basis. However, we can still measure the LZ tunneling process containing EP in diabatic basis as shown in Fig. S6. The final occupancy in band θ_l of diabatic basis ($|c_l|^2$), i.e. in the lossless band, turns out to be given by the ordinary (Hermitian) LZ formula, in spite the other band is dissipative and we cross an EP during the dynamics.

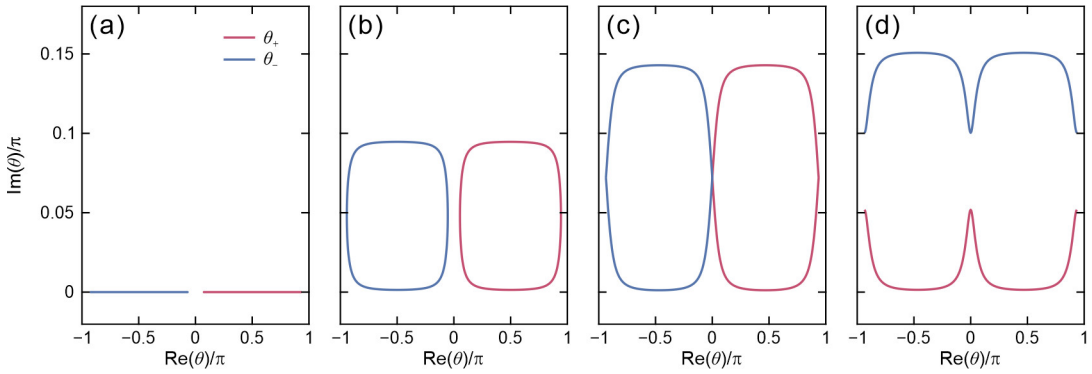

Fig. S3. Energy spectrum in complex plane for a few increasing values of loss rate γ with $\sin^2\beta = 0.05$. (a) $\gamma = 0$ for Hermitian case. (b) $\gamma = 0.3$ in the weak non-Hermitian regime. (c) $\gamma = \gamma_c$ (0.46) at the exceptional point. (d) $\gamma = 0.48$ in the strong non-Hermitian regime.

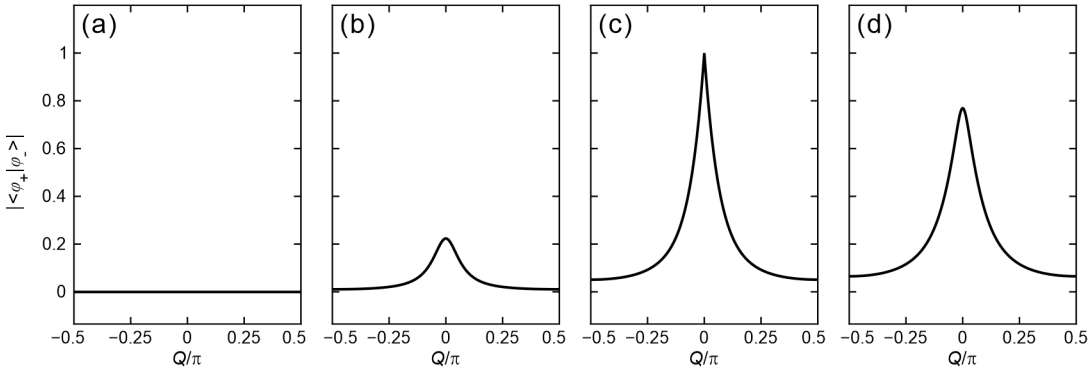

Fig. S4. The non-orthogonality of the eigenstates. (a) The overlap of the eigenstates $|\langle\varphi_+|\varphi_-\rangle|$ for $\gamma = 0$. (b-d) Same as (a) but for $\gamma = 0.1$, 0.46(γ_c), and 0.6.

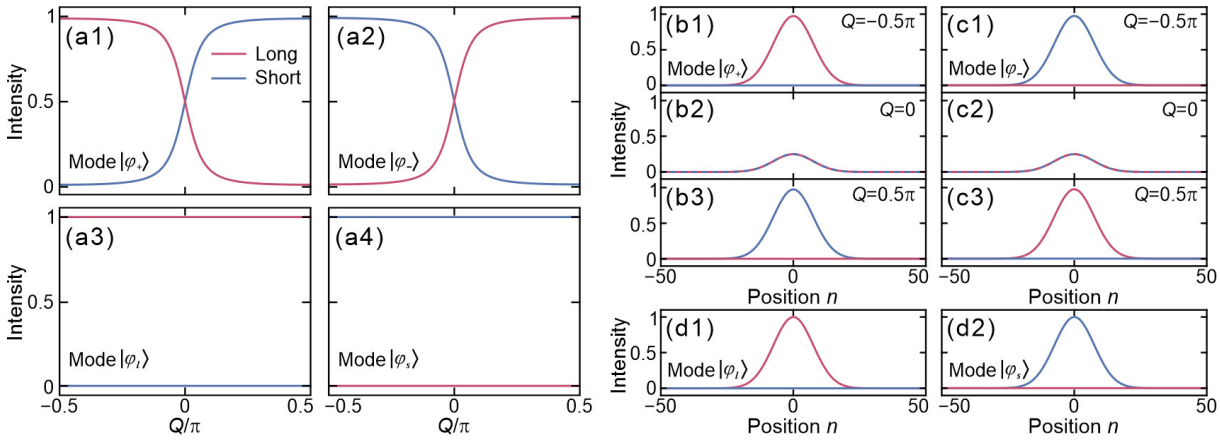

Fig. S5. Mode distributions for adiabatic and diabatic bases. (a) Mode distributions for $|\varphi_+\rangle$, $|\varphi_+\rangle$, $|\varphi_s\rangle$ and $|\varphi_l\rangle$. (b) Mode distributions with position n for state $|\varphi_+\rangle$. (c) Mode distributions with position n for the state $|\varphi_-\rangle$. (d) Mode distributions with position n for state $|\varphi_l\rangle$ and $|\varphi_s\rangle$.

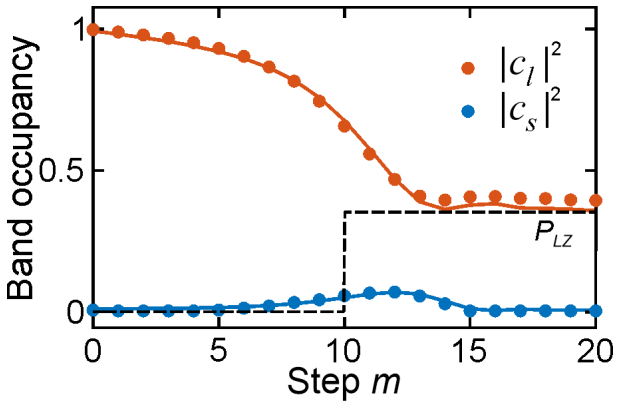

Fig. S6. Measured LZ tunneling process through EP in diabatic basis. The theoretical values are denoted by solid curves.

Supplementary Note 3: Energy splitting for completely separated modes

As mentioned in the main text, the instantaneous band occupancies can be measured by freezing the tunneling process at truncation step m_t[17]. In the presence of a strong effective electric field, the input wave packet experiences LZ tunneling between two adjacent bands. As a result, both branches of band structure are occupied. However, limited by the finite separation of two split wave packets, their intensity profiles overlap with each other during the LZ tunneling process. For truncation step m_t that is far from the avoided-crossing regions, we abruptly remove the effective electric field after the truncation step m_t. Here, the effective electric field is $E = \pi/20$, and the splitting parameter $\sin^2\beta = 0.05$. After that, the wave packets belonging to two different bands move to opposite directions in the n axis, leading to the separation of two split wave packets. By introducing the loss into the short loop, we realize the dissipative LZ tunneling. Similar to the Hermitian case, we abruptly remove the effective electric field and the loss at the same time after the truncation step m_t. Then the wave packets belonging to two different bands with opposite group velocity evolve forward till they separate from each other. The removal of the loss after truncation step m_t guarantees that the intensities of two wave packets keep equivalent during the evolution after step m_t. Figures S7(a) and S7(b) displays the above beam splitting process for $\gamma = 0$ and 0.1. One sees that the split wave packets are completely separated at step $m = 30$ in these cases. By calculating the intensities of two wave packets, we can readily obtain the band occupancies, as depicted in Figs. S7(c) and S7(d).

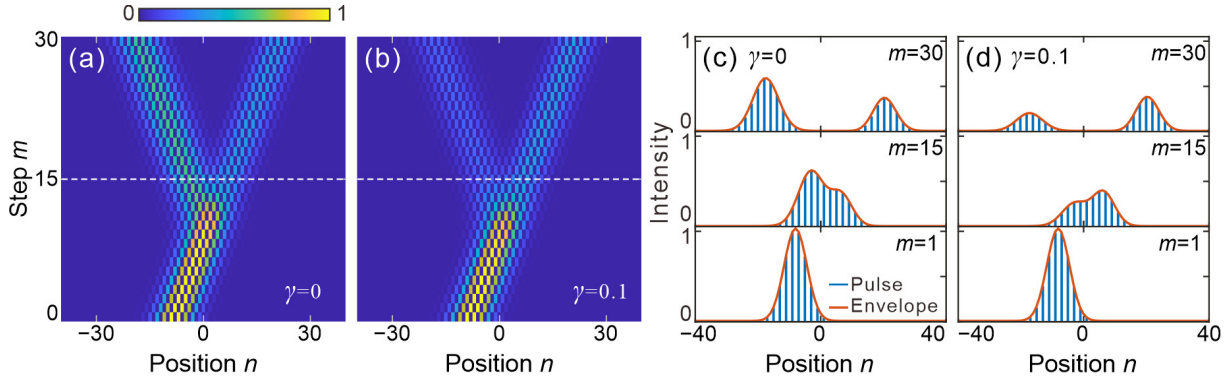

Fig. S7. Schematic diagram of energy splitting. (a), (b) Measured pulse intensity evolution with $m_t = 15$ for $\gamma = 0$ and 0.1, respectively. (c), (d) Intensity profiles of pulse trains at $m = 1$, 15, and 30 for $\gamma = 0$ and 0.1, respectively. The blue bars represent the intensity of pulses at each lattice site. The red solid lines are the corresponding fitted curves with cubic spline data interpolation.

Supplementary Note 4: Preparation of broad Gaussian wave packet

In this section, we elaborate on the non-Hermitian generation of a broad Gaussian wave packet, which enables the mode interference mentioned in the main text. The generation process contains three steps, i.e., the formation, Gaussian shaping, and eigenmode selection[67]. Firstly, a long pulse sequence is obtained by using the diffraction of a single-site excitation with non-Hermitian modulation based on Ref. 68. Specifically, this is achieved by an alternating gain-loss scheme with gain factors $G_u = \exp[(-1)^m\gamma] = 1/G_v$, where G_u and G_v correspond to short and long loops, respectively, and γ is the gain/loss parameter. As shown in Figs. S8(a) and S8(b), the gain and loss change alternately along the evolution direction and flips at every step. By using such a non-Hermitian setting, the eigenmodes in different regions of Brillouin zone will experience various degrees of gains or losses. Thus, during propagation, the spectrum will get narrower considerably. In this way, the wave transport can change from ballistic to diffusive manners. In experiment, the gain and loss are introduced by changing the transmissions of intensity modulators (IMs) in optical fiber loops. Secondly, we also use the above gain-loss scheme, but the gain/loss parameter γ is set as a smaller value compared to the one in the first part. By doing so, we can enhance the central part of the wave packet and suppress its marginal parts, leading to the Gaussian shaping of pulse sequence. As shown in Fig. S8(c), a broad Gaussian wave packet with a full width at half maximum of $\Delta n = 15$ is generated from a single pulse by utilizing the above gain-loss scheme. Finally, by implementing phase and intensity modulation onto the pulse trains in the short and long loops, we can precisely excite the eigenmode at the upper or lower band.

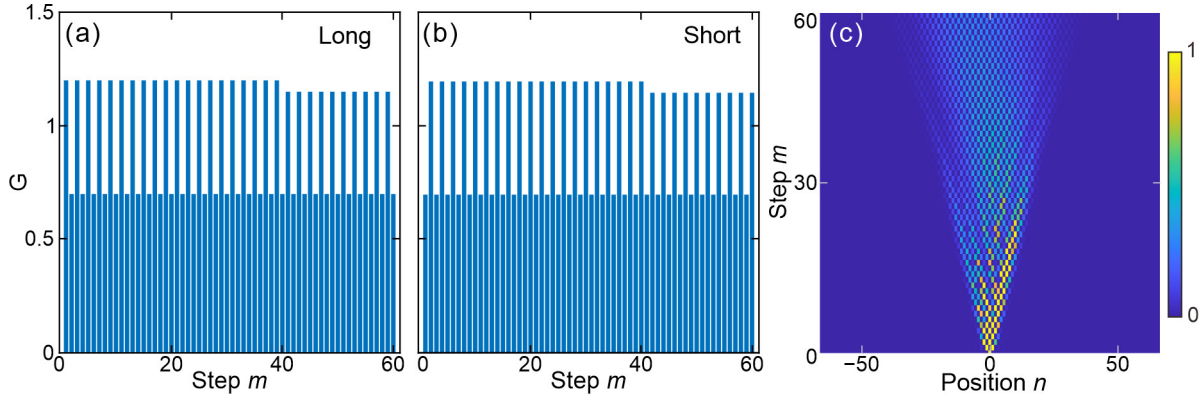

Fig. S8. Generation of broad Gaussian wave packet. (a), (b) The gain factors in long (a) and short (b) loops varying with step m. (c) Simulated pulse intensity evolution.

Supplementary Note 5: Mode interference in long and short fiber loops

A Bloch mode $|\psi\rangle$ propagating in the temporal lattice can be expressed by a superposition of upper- and lower-band modes

$$|\psi\rangle = c_+ |\varphi_+\rangle e^{i\theta_+ m} + c_- |\varphi_-\rangle e^{i(\theta_- m+\Delta\phi)}, \tag{S21}$$

where c_+ and c_- denote amplitude of upper- and lower-band modes at time step m, $\theta_\pm$ and $|\varphi_\pm\rangle$ are the eigenvalues and eigenvectors, and $\Delta\phi$ is the phase difference between the two modes. Note that the Bloch momentum $Q = 0$ and $\gamma = 0$ at this step. According to Eq. (S20), the eigenvectors belonging to the two different bands take the simple form

$$|\varphi_\pm\rangle = \begin{pmatrix} U_\pm \\ V_\pm \end{pmatrix} = \frac{1}{\sqrt{2}} \begin{pmatrix} 1 \\ \pm 1 \end{pmatrix}. \tag{S22}$$

Substituting Eq. (S22) into Eq. (S21), the intensities in the short and long loops can be calculated as

$$\begin{aligned} I_u &= \left| c_+ U_+ e^{i\theta_+ m} + c_- U_- e^{i(\theta_- m+\Delta\phi)} \right|^2 \frac{I_{m_t}}{I_0}, \\ I_v &= \left| c_+ V_+ e^{i\theta_+ m} + c_- V_- e^{i(\theta_- m+\Delta\phi)} \right|^2 \frac{I_{m_t}}{I_0}, \end{aligned} \tag{S23}$$

where I_{m_t} and I_0 is the light intensity of the time step m_t and the incident time. Further calculation leads to

$$\begin{aligned} I_u &= \frac{1}{2}\left\{ |c_+|^2 + |c_-|^2 + |c_+ c_-| \left[e^{i(\theta_+ - \theta_-)m - i\Delta\phi} + c.c. \right] \right\} \frac{I_{m_t}}{I_0}, \\ I_v &= \frac{1}{2}\left\{ |c_+|^2 + |c_-|^2 - |c_+ c_-| \left[e^{i(\theta_+ - \theta_-)m - i\Delta\phi} + c.c. \right] \right\} \frac{I_{m_t}}{I_0}. \end{aligned} \tag{S24}$$

The above intensities can be further expressed as

$$\begin{aligned} I_u &= \left\{ \frac{1}{2}\left(|c_+|^2 + |c_-|^2 \right) + |c_+ c_-| \cos\left[(\theta_+ - \theta_-)m + \Delta\phi \right] \right\} \frac{I_{m_t}}{I_0}, \\ I_v &= \left\{ \frac{1}{2}\left(|c_+|^2 + |c_-|^2 \right) - |c_+ c_-| \cos\left[(\theta_+ - \theta_-)m + \Delta\phi \right] \right\} \frac{I_{m_t}}{I_0}. \end{aligned} \tag{S25}$$

According to the band structure $\theta_\pm = \pm \cos^{-1}[\cos(\beta)\cos(Q + i\gamma/2)] + i\gamma/2$, we have $\theta_+ - \theta_- = 2\beta$ when $Q = 0$ and $\gamma = 0$. Then, the intensities are given by

$$\begin{aligned} I_u &= \left\{ \frac{1}{2}\left(|c_+|^2 + |c_-|^2 \right) + |c_+ c_-| \cos\left[2\beta m + \Delta\phi \right] \right\} \frac{I_{m_t}}{I_0}, \\ I_v &= \left\{ \frac{1}{2}\left(|c_+|^2 + |c_-|^2 \right) - |c_+ c_-| \cos\left[2\beta m + \Delta\phi \right] \right\} \frac{I_{m_t}}{I_0}. \end{aligned} \tag{S26}$$

From Eq. (S26), one sees that interference fringes appear both in the short and long loops. Furthermore,

the two interference fringes have identical period and bias, which equal to $T = \pi/\beta$ and $(|c_+|^2+|c_-|^2)/2$, respectively. More interestingly, the two interference fringes are out-of-phase. However, in realistic experiment, it is very hard to generate an infinite Bloch eigenmode.

Here, we prepare a broad Gaussian wave packet with $\Delta n = 15$ to simulate the behavior of Bloch eigenmode. As illustrated in Figs. S9(a) and S9(b), we can also observe clear interference fringes in the short and long loops by using the broad wave packet. Furthermore, the time step where the fringes show the constructive interference in short loop is exactly the one where the destructive interference emerges in long loop. To further analyze the interference fringes, the total light energies in the short and long loops varying with step m are shown in Figs. S9(c) and S9(d). By doing so, we can extract all information of interference patterns, such as contrast ratios and initial phases, which reflect the coefficients of two eigenmodes.

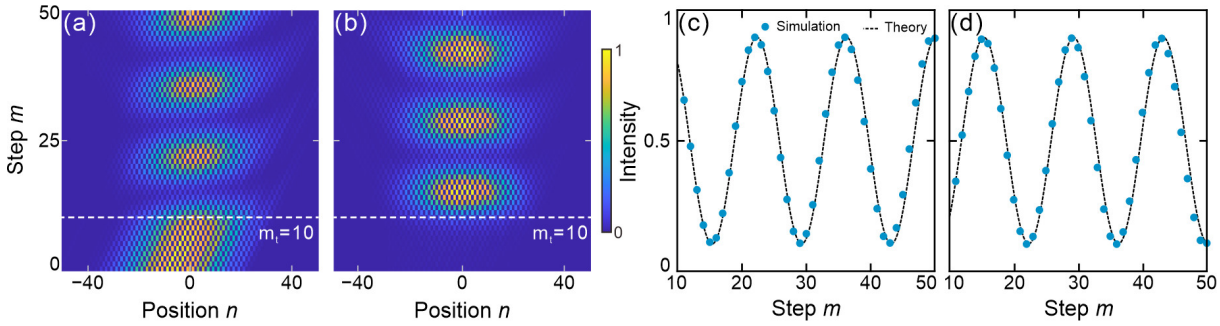

Fig. S9. Interference in long and short loops. (a), (b) Simulated pulse intensity evolutions for $m_t = 10$ in short and long loops, respectively. (c), (d) Total light energies varying with step m in short and long loops. All have $\sin^2(\beta) = 0.05$, $E = \pi/20$, and $\gamma = 0.1$.

Supplementary Note 6: Mode recovering after abrupt change of gauge potential

Considering the evolution of the time steps from m_t to $m_t + 1$ as $|\psi\rangle = \Gamma|\psi'\rangle$, where $|\psi\rangle$ and $|\psi'\rangle$ are wavefunctions of the step after the truncation (m_t+1) and the truncating time step m_t. The wavefunction $|\psi'\rangle$ of the time step m_t can be expanded in the eigenvectors $|\psi'\rangle = c'_+|\varphi'_+\rangle + c'_-|\varphi'_-\rangle$ and the eigenvectors $|\varphi'_\pm\rangle$ can be obtained by Eq. (S20). Therefore, we can derive the spectral amplitudes of time step m_t as

$$|\psi'\rangle = M'\begin{pmatrix} c'_+ \\ c'_- \end{pmatrix} = \begin{pmatrix} U'_+ & U'_- \\ V'_+ & V'_- \end{pmatrix}\begin{pmatrix} c'_+ \\ c'_- \end{pmatrix}. \tag{S27}$$

The corresponding time propagator in Q-space is deduced from Eq. (S10)

$$\Gamma(Q) = \begin{pmatrix} \cos(\beta)e^{i\Phi} & i\sin(\beta)e^{i\Phi} \\ i\sin(\beta)e^{-i\Phi} & \cos(\beta)e^{-i\Phi} \end{pmatrix}. \tag{S28}$$

where $\Phi = Q + \Delta\phi$, representing the Bloch momentum at time step $m_t + 1$ after the variation of gauge potential. As if $\Delta\phi = E$, the effective electric field keeps constant at time step $m_t + 1$. Else if $\Delta\phi = 0$, the effective field is removed although the gauge potential keeps unchanged. For a special case $\Delta\phi = -Q$, that is, $\Phi = 0$, the Bloch momentum of the modes equals to that at the crossing point, which suggests the group velocities of the modes should have the same directions. Under this circumstance, the modes belonging to distinct bands could undergo a perfect interference.

At the time step $m_t + 1$, the Bloch mode can also be expanded by the eigenvectors of the two bands $|\psi\rangle = c_+|\varphi_+\rangle + c_-|\varphi_-\rangle$ with $c_\pm$ being the mode coefficients obtained in experiment and $|\varphi_\pm\rangle$ can be obtained by Eq. (S20). Therefore, we can derive the spectral amplitudes of time step m_t+1 as

$$|\psi\rangle = M\begin{pmatrix} c_+ \\ c_- \end{pmatrix} = \begin{pmatrix} U_+ & U_- \\ V_+ & V_- \end{pmatrix}\begin{pmatrix} c_+ \\ c_- \end{pmatrix}. \tag{S29}$$

With transfer matrix $\Gamma(Q)$ in Eq. (S28), the relation $|\psi\rangle = \Gamma|\psi'\rangle$ can be expressed as $M(c_+, c_-)^T = \Gamma M'(c'_+, c'_-)^T$. Thus, the relation of mode coefficients corresponding to m_t and $m_t + 1$ can be obtained as $(c'_+, c'_-)^T = M'^{-1}\Gamma^{-1}M\,(c_+, c_-)^T$, which can be further expressed as

$$\begin{pmatrix} c'_+ \\ c'_- \end{pmatrix} = \begin{pmatrix} U'_+ & U'_- \\ V'_+ & V'_- \end{pmatrix}^{-1}\begin{pmatrix} \cos(\beta)e^{i\Phi} & i\sin(\beta)e^{i\Phi} \\ i\sin(\beta)e^{-i\Phi} & \cos(\beta)e^{-i\Phi} \end{pmatrix}^{-1}\begin{pmatrix} U_+ & U_- \\ V_+ & V_- \end{pmatrix}\begin{pmatrix} c_+ \\ c_- \end{pmatrix}. \tag{S30}$$

When applying an abrupt change of gauge potential $\Delta\phi = -Q$ so as to $\Phi = 0$, we have

$$\Gamma = \begin{pmatrix} \cos(\beta) & i\sin(\beta) \\ i\sin(\beta) & \cos(\beta) \end{pmatrix}. \tag{S31}$$

The corresponding inverse matrix is

$$\Gamma^{-1} = \begin{pmatrix} \cos(\beta) & -i\sin(\beta) \\ -i\sin(\beta) & \cos(\beta) \end{pmatrix}. \tag{S32}$$

And we have $|\varphi_{\pm}\rangle = 1/\sqrt{2}\,(1,\pm 1)^{T}$. Thus matrix M can take the simple form

$$M = \begin{pmatrix} U_{+} & U_{-} \\ V_{+} & V_{-} \end{pmatrix} = \frac{1}{\sqrt{2}} \begin{pmatrix} 1 & 1 \\ 1 & -1 \end{pmatrix}. \tag{S33}$$

Further, we have

$$\Gamma^{-1} M = \begin{pmatrix} e^{-i\beta} & e^{i\beta} \\ e^{-i\beta} & -e^{i\beta} \end{pmatrix}. \tag{S34}$$

Note that the matrix M' is not a unitary matrix, we utilize the left eigenvectors in Eq. (S20) to obtain the identity matrix

$$\begin{pmatrix} \hat{U}'^{*}_{+} & \hat{V}'^{*}_{+} \\ \hat{U}'^{*}_{-} & \hat{V}'^{*}_{-} \end{pmatrix} \begin{pmatrix} U'_{+} & U'_{-} \\ V'_{+} & V'_{-} \end{pmatrix} = \begin{pmatrix} \langle \chi'_{+} | \varphi'_{+} \rangle & \langle \chi'_{+} | \varphi'_{-} \rangle \\ \langle \chi'_{-} | \varphi'_{+} \rangle & \langle \chi'_{-} | \varphi'_{-} \rangle \end{pmatrix} = \begin{pmatrix} 1 & 0 \\ 0 & 1 \end{pmatrix}. \tag{S35}$$

The matrix M'^{-1} can be expressed as

$$M'^{-1} = \begin{pmatrix} U'_{+} & U'_{-} \\ V'_{+} & V'_{-} \end{pmatrix}^{-1} = \begin{pmatrix} \hat{U}'^{*}_{+} & \hat{V}'^{*}_{+} \\ \hat{U}'^{*}_{-} & \hat{V}'^{*}_{-} \end{pmatrix}. \tag{S36}$$

Finally, we can establish the relation between the mode coefficients at adjacent time steps

$$\begin{pmatrix} c'_{+} \\ c'_{-} \end{pmatrix} = \frac{1}{\sqrt{2}} \begin{pmatrix} \hat{U}'^{*}_{+} & \hat{V}'^{*}_{+} \\ \hat{U}'^{*}_{-} & \hat{V}'^{*}_{-} \end{pmatrix} \begin{pmatrix} e^{-i\beta} & e^{i\beta} \\ e^{-i\beta} & -e^{i\beta} \end{pmatrix} \begin{pmatrix} c_{+} \\ c_{-} \end{pmatrix}. \tag{S37}$$

As far as $c_{\pm}$ are obtained by fitting the interference pattern in the experiment, we can achieve the coefficients $c'_{\pm}$ at time step m_t.